Coupling organic free-radical molecules to lumped-element superconducting resonators

M. Rubín-Osanz,[1] M. C. de Ory,[2] I. Gimeno,[1] D. Granados,[3] D. Zueco,[1] A. Gomez,[2] and F. Luis[1]

[1] *Instituto de Nanociencia y Materiales de Aragón (INMA), CSIC-Universidad de Zaragoza, Zaragoza 50009, Spain*
[2] *Centro de Astrobiología (CAB),CSIC-INTA, Torrejón de Ardoz 28850, Spain*
[3] *IMDEA-Nanociencia, Madrid 28049, Spain*

A promising route towards the realization of a molecular spin quantum processor relies on coupling magnetic molecules to individual photons confined within superconducting resonators. As a simple approximation to such a hybrid scheme, here we explore the conditions that determine the collective coupling of DPPH organic free radicals to lumped-element LC superconducting resonators. In these chips, multiple resonators are coupled to a single readout line. This enables designing the relevant resonator properties, such as resonance frequency, cavity volume and impedance, while keeping a perfect transmission for the device. Here, we exploit these design possibilities to achieve the coherent spin-photon coupling regime. Besides, we study how this coupling depends on the relative orientation of the external dc magnetic field with respect to the photon magnetic field and on the spins locations with respect to the chip surface.

I. INTRODUCTION

Magnetic molecules are seen as potentially advantageous physical realization of spin qubits, due to their easily controllable purity and reproducibility, and to the fact that the individual qubit properties can be tuned by chemistry.[1–3] Besides helping to shield the spins from magnetic noise,[4–8] molecular design also gives opportunities for encoding multiple qubits within each molecule.[9–19] However, wiring up such molecules into a large scale quantum computing architecture, able to take on computational problems of practical interest, remains very challenging.

Recent proposals aim at exploiting techniques and protocols developed for superconducting quantum processors,[20–23] but adapting them to the molecular size and to the fact that their spins couple to the photon magnetic field.[24–26] The idea is to use the coupling of the molecular spins to superconducting resonators in order to readout the spin states[27] and to introduce the effective interactions between remote molecules[19,26,28] that are key to achieve full scalability. The first proposals[24,25] were based on coplanar resonators.[29] These are fabricated by interrupting a superconducting transmission line to create a cavity with a length matching the wavelength of microwave photons. However, this design limits the tuneability of the resonator frequency $\omega_{\rm r} = 1/\sqrt{LC}$, because its capacitance C and inductance L must be tailored in order to match the transmission line impedance ($Z = \sqrt{L/C}$).

Lumped-element resonators (LERs) allow avoiding some the shortcomings of the coplanar resonator design. A LER is an LC resonating circuit side-coupled to a readout transmission line, consisting of an inductive meander and an inter-digitated capacitor. This means that its impedance does not need to match the line impedance, thereby allowing an independent tuning of the inductance and capacitance of the LER, and therefore its resonance frequency, by changing the design of the inductor and the capacitor. On top of that, they achieve very high quality factors ($Q \sim 10^4$ to 10^5) and, therefore, long photon coherence times (¿ μs). Another important property of LERs is their frequency multiplexing. A LER only absorbs microwave signals in the transmission line with frequencies in its bandwidth, making it effectively transparent to other signals. As a consequence, several LERs with different resonance frequencies can be measured by coupling them to a single transmission line.

While coplanar resonators have been already used to reach the strong coupling regime with molecular spin ensembles,[30–32] with LERs this regime has been achieved only with samples of non-molecular spins.[33] Here we explore the coupling to LERs of ensembles of the simplest molecular spin qubits, organic free radicals hosting an unpaired electron with $S = 1/2$ and $g_S \simeq 2$. The experiments illustrate the basic characteristics of a hybrid spin-LER platform and which parameters determine its main ingredient, the spin-photon coupling.

II. EXPERIMENTAL SETUP

Two superconducting chips were fabricated. They are made of 100 nm thick Nb films deposited by DC magnetron sputtering on top of 275 μm thick Si substrate wafers. Each chip hosts twelve LERs with resonance frequencies ranging between 1.5 and 2.1 GHz and different geometries. All of them are side-coupled to the same transmission line as shown in Fig. 1a-b.

Transmission experiments were carried out at 4.2 K, inserting a probe with the chip in a ^{4}He cryostat equipped with a 9/1/1 T vector magnet. This set-up allows applying dc magnetic fields with amplitudes B up to 1 T along any arbitrary direction in the X, Y, Z laboratory reference frame shown in Fig. 1c. In these experiments, $\vec{B}$ was rotated within the $X-Y$ plane of the device. The

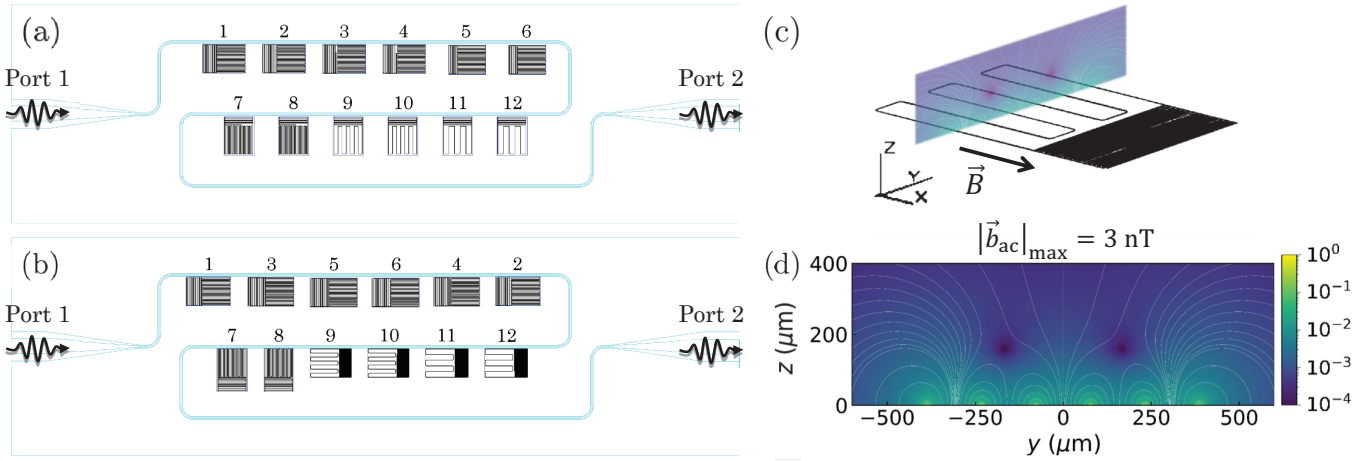

FIG. 1. **Superconducting chips and lumped-element resonators. a-b**: Schemes of the two superconducting chips used in the microwave transmission experiments. **c-d**: Simulation of the distribution of microwave magnetic fields generated above the LER inductor by the vacuum fluctuations of the resonator in resonance.

chip was connected to the outside electronics with stainless steel semi-rigid coaxial lines. Microwave transmission measurements were performed with a Vector Network Analyzer (VNA). In all plots that follow, the microwave transmission S_{21} is normalized by the transmission that the line has when it is not in resonance with the LERs.

The organic free radical used in these experiments is 2,2-diphenyl-1-picrylhydrazyl (DPPH), a widely used standard in Electron Paramagnetic Resonance (EPR).[34] Samples are DPPH in powder form, as purchased from Sigma Aldrich (reference D9132), pressed into pellets and deposited on top of the LER inductor. The pellets have a thickness of ∼100 μm and an area (∼ 1 mm^2) slightly larger than the LER size, covering the whole inductor. They were fixed with a thin layer of paratone oil. The $S = 1/2$ free radical spin behaves nearly as the spin of a free electron. Therefore, it is described by the simple spin Hamiltonian:

$$\mathcal{H} = \frac{\mu_B g_S B}{2}\hat{\sigma}_z = \frac{\hbar\omega_q}{2}\hat{\sigma}_z, \tag{1}$$

with a g-factor $g_S = 2.004$ just above the value for a free electron.[35] The static magnetic field $\vec{B}$ allows tuning the spin transition frequency $\omega_q = \mu_B g_S B/\hbar$.

The spin-photon coupling arises from the modulation of the Zeeman interaction in (1) by the microwave magnetic field $\vec{b}_{ac}$ associated to vacuum fluctuations in the resonator. As Fig. 1c shows, this field is mainly confined within a plane perpendicular to the longer LER inductor lines. The coupling $G_{1,j}$ of each molecular spin j is proportional to the component of $\vec{b}_{ac}$ that is perpendicular to $\vec{B}$.[24] Figure 1d shows the distribution of $|\vec{b}_{ac}|$ in the plane included in Fig. 1c, normalized by the maximum $|\vec{b}_{ac}|$.

III. STRONG COLLECTIVE SPIN-PHOTON COUPLING WITH A LER

LERs 1 to 6 in the chip of Fig. 1a share a similar design, with slightly different frequencies tuned by small changes in their capacitor sizes. The transmission of the chip was measured for microwave input signals with frequencies close to the resonance frequency ω_r of LERs 1, 3 and 5. The same DPPH sample was moved from one resonator to the next between experiments, see Fig. 2a-b. Figure 2c shows results measured for different magnetic fields. The coupling between the spins and each resonator mode becomes apparent when the field-dependent spin transition frequency ω_q gets close to ω_r. The spin-photon resonance field B_{res} is defined by the condition $\omega_r = \omega_q = \mu_B g_S B_{res}/\hbar$.

The experiments are modeled using input-output theory for the transmission S_{21} through the readout line. The model considers an external microwave driving signal with frequency ω_d, which is fed into the system via port 1 and that excites a resonator coupled to an ensemble of non-interacting spins. This leads to the following expression for S_{21}:[36]

$$S_{21}(\omega_d) = 1 - \frac{\kappa_c}{i(\omega_r - \omega_d) + \kappa + \dfrac{G_N^2 \Delta P}{i(\omega_q - \omega_d) + \gamma_\perp}}, \tag{2}$$

Here, κ_c is the coupling rate between the transmission line and the resonator, κ and $\gamma_\perp$ are the photon and spin decoherence rates, respectively, $\Delta P = \tanh(\hbar\omega_q/k_B T)$ is the population difference between the spin down and spin up states at temperature T, and G_N is the collective spin-photon coupling:

$$G_N = \sqrt{\sum_{j=1}^{N} |G_{1,j}|^2}, \tag{3}$$

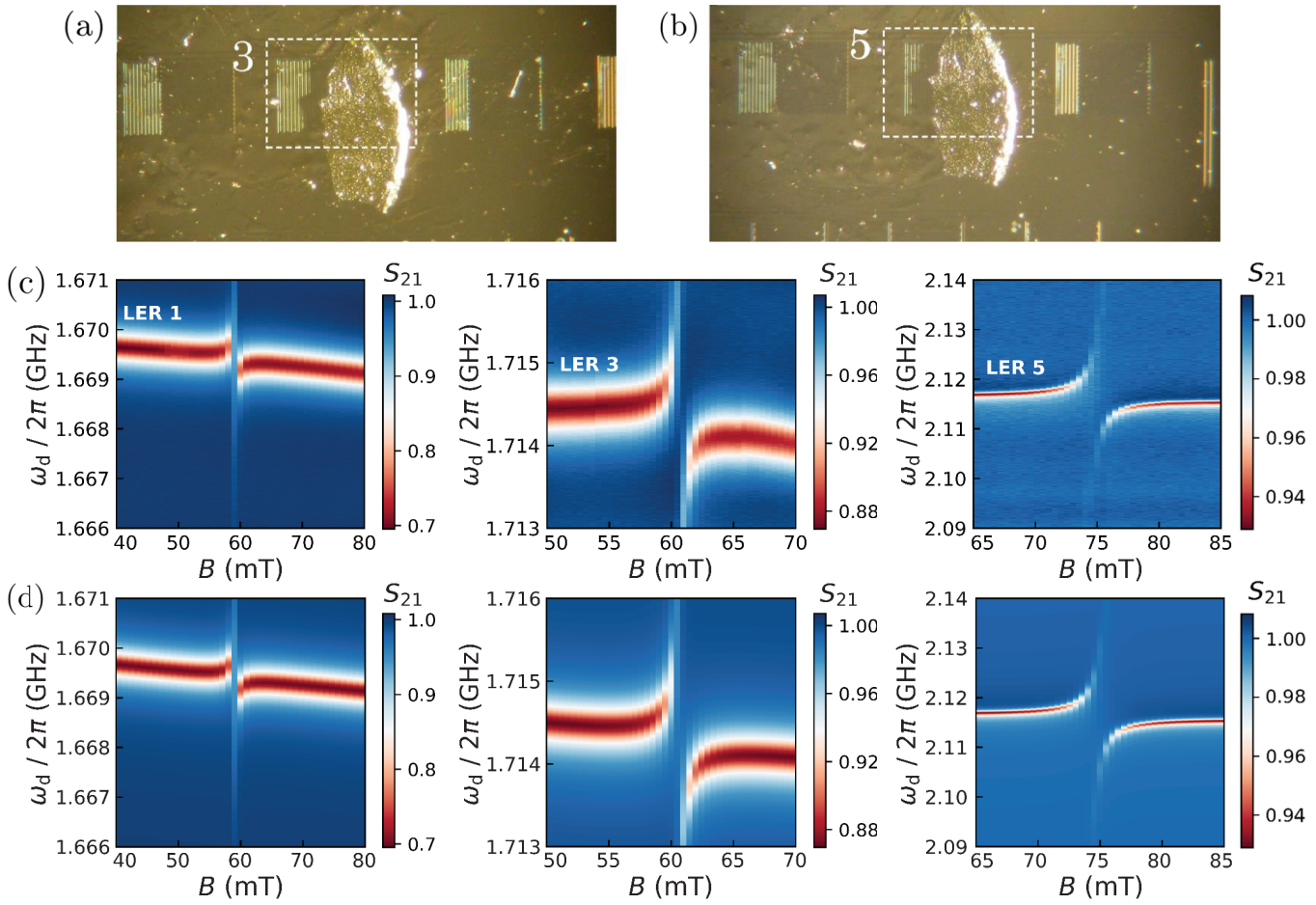

FIG. 2. **Coupling of DPPH powder samples to lumped-element resonators. a-b**: Optical microscopy image of a DPPH pellet located on top of the inductors of LER 3 (a) and LER 5 (b). The same sample was moved from LER 1 to LER 3 and then to LER 5. **c**: Microwave transmission S_{21} measured for driving frequencies close to the resonance frequencies of LERs 1, 3 and 5 and static magnetic fields B around the spin-photon resonance condition $\omega_r = \omega_q = \mu_B g_S B_{res}/\hbar$. **d**: Least-square fits of the experimental data based on Eq. (2).

which becomes enhanced with respect to the coupling of each individual spin by $\sim \sqrt{N}$, where N is the number of free radical molecules in the sample. This description is valid as long as N is much larger than the number n of photons in the resonator, which is ensured by using large, fully concentrated DPPH samples with $N \sim 10^{17}$ spins and sufficiently low input microwave power. In what follows, ΔP is included in the spin-photon coupling by defining a temperature-dependent effective $G_N \propto \sqrt{\Delta P}$. Figure 2d shows least-square fits of the transmission data based on Eq. (3). These fits allow the determination of G_N, κ and $\gamma_\perp$ from each experimental curve.

The strong collective coupling regime is defined by the condition $G_N > \gamma_\perp$ and κ. In our case, $\gamma_\perp \gg \kappa$, thus it is the spin decoherence rate that defines the threshold for the spin-photon coupling. This limit is achieved only when the sample is coupled to LER 5. Then $G_N/2\pi = 12.491 \pm 0.004$ MHz and $\gamma_\perp/2\pi = 6.5 \pm 0.5$ MHz, which gives $G_N/\gamma_\perp = 1.9 \pm 0.1$. Transmission data measured for magnetic fields close to the resonance field B_{res} show the two minima that correspond to the excitation of the two polaritonic states of this hybrid system. These states are quantum superpositions of photon and spin excitations, with transition frequencies:[20]

$$\omega_\pm = \omega_r + \frac{\Delta}{2} \pm \sqrt{\left(\frac{\Delta}{2}\right)^2 + G_N^2}, \qquad (4)$$

where $\Delta = \omega_q - \omega_r$ is the detuning between the spin and photon frequencies. The magnetic field dependence of ω_+ and ω_- is shown in Fig. 3a. Figure 3b shows that the two transmission minima become visible for $|\Delta|/G_N \lesssim 1$.

The collective couplings obtained with LERs 1 and 3, $G_N/2\pi = 2.586 \pm 0.003$ MHz and $G_N/2\pi = 3.758 \pm 0.003$ MHz, respectively, are smaller than that found for LER 5. These values were extracted by fitting the transmission data with the same $\gamma_\perp$, which is intrinsic to the sample. Even though the strong coupling is not achieved in these two cases, the high cooperativity regime is attained for the three LERs. This regime is defined by a cooperativ-

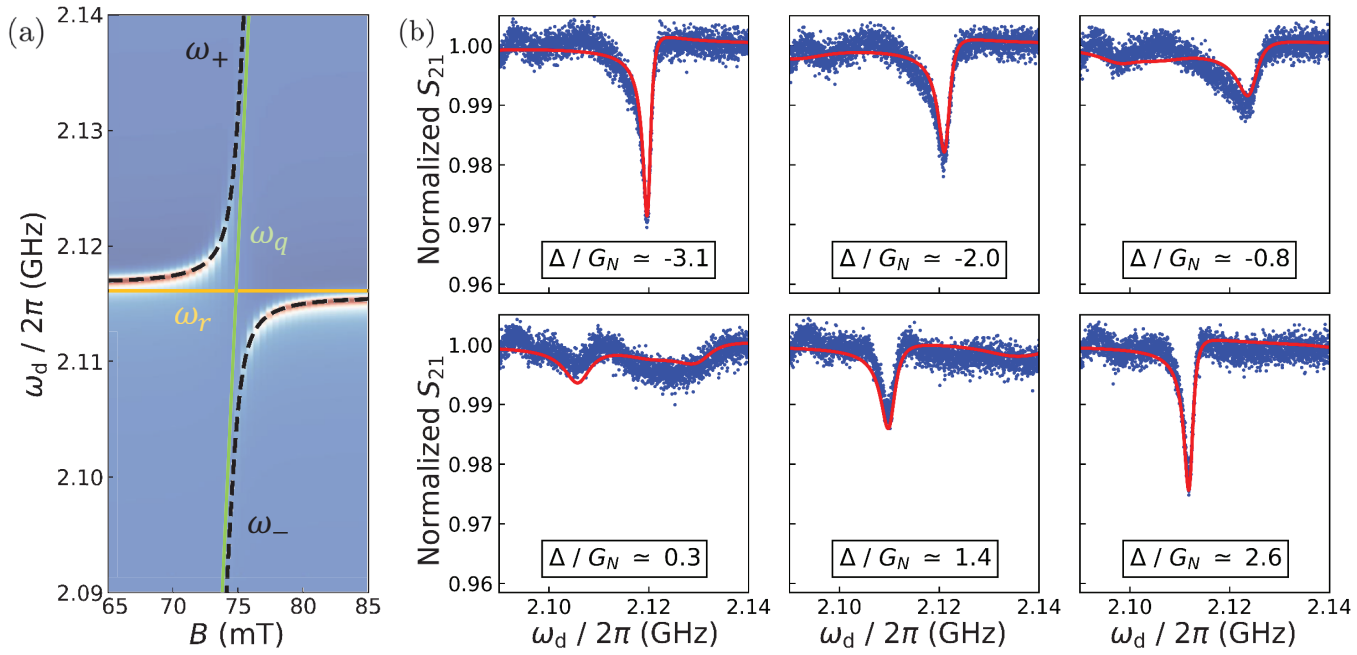

FIG. 3. **Strong coupling of a DPPH powder sample to LER 5.** **a**: Microwave transmission measured for driving frequencies close to the resonance frequency of LER 5 and for static magnetic fields B around the spin-photon resonance condition $\omega_r = \omega_q = \mu_B g_S B_{res}/\hbar$. Dashed black lines show the frequencies of the spin-photon polaritonic excitations, as given by Eq. (4). **b**: Transmission data measured at six values of $\Delta = \omega_q - \omega_r$ (different magnetic fields). Two transmission minima are observed for $|\Delta|/G_N \lesssim 1$.

ity $C \equiv G_N^2/\gamma_\perp\kappa > 1$. With $\kappa/2\pi$ ranging between 200 and 500 kHz for these resonator designs at $T = 4.2$ K, we find $C = 4.0 \pm 0.3$ for LER 1, $C = 10.6 \pm 0.8$ for LER 3, and $C = 57.9 \pm 4.5$ for LER 5. Within this limit, at resonance nearly every photon in the cavity is coherently transferred to the spin ensemble. It also provides the necessary condition to determine the spin state by reading out ω_r in the dispersive limit $|\Delta| \gg G_N$.[27]

The results described above show that G_N gets higher as the same sample is moved from LER 1 to LER 3 and from the latter to LER 5. Since we are dealing with the same DPPH pellet in all cases (see Fig. 2a-b), the changes observed in G_N must be associated with differences in the microwave fields $\vec{b}_{ac}$ felt by the spins. Its intensity scales with the square root of the resonance frequency ω_r,[33] which does increase from LER1 to LER 5 (see Fig. 2b). However, this effect alone cannot explain the change in G_N. Let us take the resonators with highest (LER 5) and lowest (LER 1) spin-resonator coupling. The difference between their resonance frequencies accounts for an increase by a factor 1.13 in G_N, whereas the experiments show that G_N is enhanced by a factor 4.83. This suggests that other experimental parameters, in particular the location of the spins with respect to each resonator, may have a larger, dominant effect.

The position of the sample determines how much of the resonator mode volume, the region of space with a non-negligible $\vec{b}_{ac}$, is actually filled with spins. The three resonators share the same inductor design, which leads to a very similar spatial distribution of $\vec{b}_{ac}$. In the experiments described above, the DPPH pellet covered completely the $X-Y$ area defined by the inductor. Therefore, the differences observed experimentally likely arise from the distance along the Z axis. As Fig. 1d shows, the intensity of $\vec{b}_{ac}$ decays very rapidly with increasing z away from the surface.[24] Any irregularities in the sample, as well as the layer of oil that sticks it to the chip surface, contribute to create a gap of the order of a few micrometres at the chip-sample interface.[37] The rapid increase in G_N suggests that the chip-sample gap was closing as the sample was moved from the first resonator (LER 1) to the last one (LER 5). This interpretation is illustrated by Fig. 4a. When the sample is moved from one LER to the next, it leaves behind part of the oil layer. The gap can be estimated by simulating G_N for different values of the chip to sample distance and comparing the result with the G_N values obtained experimentally. This is shown in Fig. 4b. We see that the increase in G_N is compatible with the DPPH sample getting closer to the chip. The ~ 12.5 μm gap in LER 5 might be associated to irregularities in the sample surface.

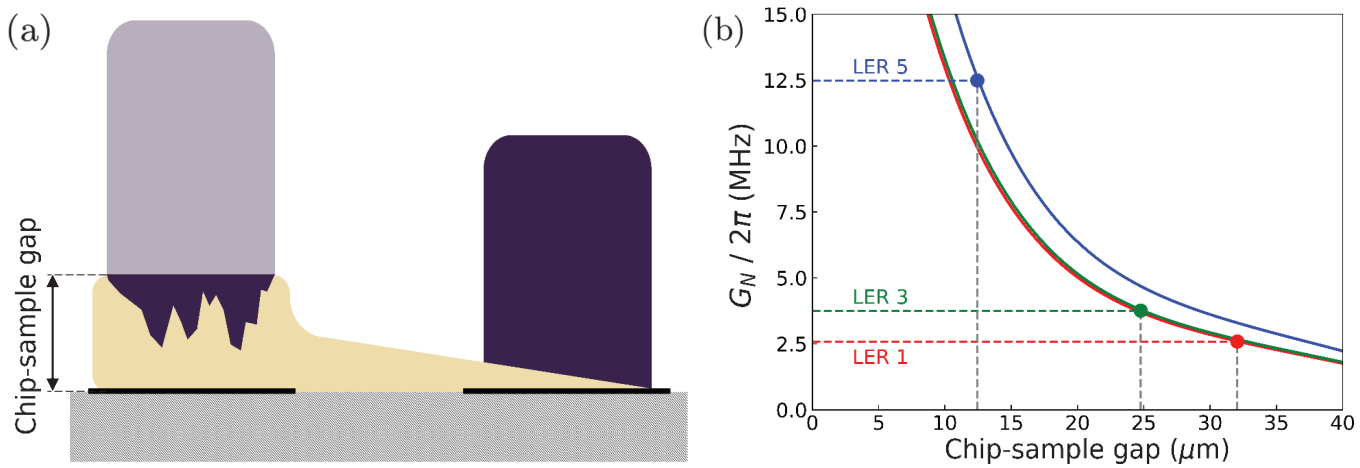

FIG. 4. **Effect of the chip-sample gap on the collective spin-photon coupling.** **a**: Sketch of how the chip-sample gap decreases as the sample is moved from one LER (left) to the next (right). The oil layer between the sample and the chip is partially left behind, thus reducing the gap between the two. **b**: Simulation of G_N for LERs 1, 3 and 5 with different chip-sample gaps. We assume that the rest of the resonator mode-volume is filled by the large DPPH sample. A comparison with the experimental G_N values (horizontal dashed lines) gives an estimation of the gap in each resonator (vertical dashed lines): ~ 32 μm in LER 1, ~ 25 μm in LER 3, and ~ 12.5 μm in LER 5.

IV. EFFECT OF THE MAGNETIC FIELD ORIENTATION ON THE SPIN-PHOTON COUPLING

In what follows, we consider experiments performed with LER 7 of the chip sketched in Fig. 1a. This LER allows studying a different geometry, with the longer inductor lines perpendicular to the readout transmission line. Its design is similar to that of LERs 1, 3 and 5, just rotated by 90°. The microwave magnetic field $\vec{b}_{\rm ac}$ generated by the inductor of LER 7 has then some components parallel to the transmission line, which we call the chip axis. If the static field $\vec{B}$, which according to Eq. (1) fully determines the spin quantization axis, is applied along the chip axis as in the previous experiments, these 'longitudinal' components of $\vec{b}_{\rm ac}$ do not contribute to G_N. This effect can be observed by measuring G_N for different orientations of $\vec{B}$.

A large DPPH sample was deposited on LER 7, as shown in Fig. 5a, covering the whole resonator area. The static magnetic field $\vec{B}$ was rotated within the plane of the chip (Fig. 5b). The microwave transmission was measured for five angles $0 \leq \theta \leq \pi/2$ between $\vec{B}$ and the chip axis. The results are shown in Fig. 5c.

The collective spin-photon coupling G_N determined from these data increases as the magnetic field is rotated from $\theta = 0$, when it is parallel to the chip axis, towards $\theta = \pi/2$, when it is parallel to the resonator inductor lines. It is easy to understand that the latter orientation gives the maximum G_N, because almost all the microwave field $\vec{b}_{\rm ac}$ generated by the inductor lies then in a plane perpendicular to $\vec{B}$. Conversely, for $\theta = 0$ only the components of $\vec{b}_{\rm ac}$ perpendicular to the chip contribute to the coupling. If the whole resonator mode is covered by the sample, the in-plane and out-of-plane components of $\vec{b}_{\rm ac}$ contribute equally to the collective coupling. Then, from the definition of G_N in Eq. (3), it follows that the out-of-plane $\vec{b}_{\rm ac}$ accounts for $1/\sqrt{2}$ ($\sim$70%) of the maximum G_N. This simple model describes very well the dependence of G_N on θ, as Fig. 5e shows.

The possibility of tuning G_N in situ by rotating the magnetic field allows detecting the direct coupling of the DPPH spins to the readout line. The coupling to the line becomes clearly visible for $\theta = 0$ and $\theta = \pi/8$, see Fig. 5c, for which the coupling to the resonator is close to its minimum. This signal enables characterizing the spin qubit frequency away from the resonance condition $\omega_{\rm q} = \omega_{\rm r}$. Besides, it is relevant for the future implementation of a quantum computing platform with molecular spins, because the line can provide the means to control the spin states while the resonator is not tuned to the qubit frequency, i.e., when $|\Delta| > 0$.[26,38]

V. INHOMOGENEITY IN THE SPIN-PHOTON COUPLING

In this section, we explore in more detail a further consequence of the strong spatial variation of $\vec{b}_{\rm ac}$. For this, we use the chip sketched in Fig. 1b. This chip has pairs of LERs with the same design and very close frequencies (just a few MHz separate their respective $\omega_{\rm r}$ values). These pairs are formed by LERs 1 and 2, LERs 3 and 4, and LERs 5 and 6 in the top row, and LERs 7 and 8, LERs 9 and 10, and LERs 11 and 12 in the bottom row. DPPH samples were first deposited on one resonator of each pair, then moved to the previously empty one.

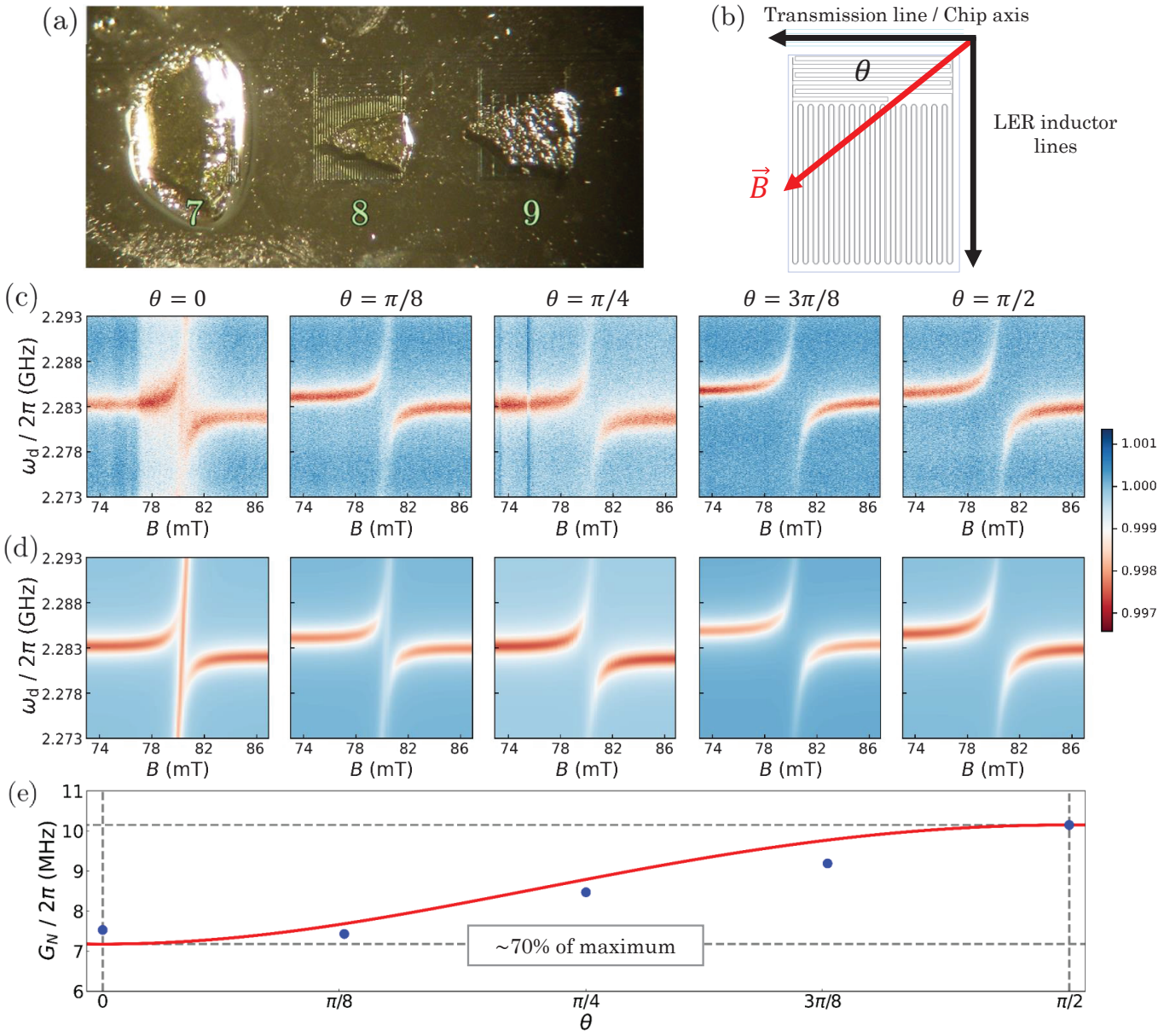

FIG. 5. **Transmission experiments for different magnetic field orientations.** **a**: Optical microscopy images of LERs 7, 8 and 9 of the chip sketched in Fig. 1a. LER 7 hosts the largest DPPH sample, covering the whole resonator mode volume. This resonator was chosen for the transmission experiments with different magnetic field orientations. **b**: Orientation of the static magnetic field $\vec{B}$ in a reference frame formed by the chip axis, defined by the transmission line, and the longer inductor lines of LER 7. **c**, Chip transmission for driving frequencies close to ω_r of LER 7, measured for magnetic fields around the spin-photon resonance condition $\omega_r = \omega_q = \mu_B g_S B_{res}/\hbar$ and different orientations, as indicated. **d**: Fit of the experimental data with Eq. (2). **e**: Evolution of the collective spin-photon coupling G_N with angle θ (blue dots). The red solid line shows G_N calculated for a DPPH sample covering the whole resonator mode volume.

In what follows, we focus on the results obtained with the pair formed by LERs 7 and 8, although the other pairs showed a very similar behaviour. First, the DPPH sample was deposited on top of LER 8 (Fig. 6a) and then, as shown in Fig. 6b, it was moved to LER 7. The transmission measured in the first experiment for frequencies $\sim \omega_r$ of LER 8 is shown in Fig. 6c, while the transmission measured after moving the sample is shown in Fig. 6d. In the latter case, signatures of the coupling to spins are observed not only for LER 7, as it is natural, but also for the 'nominally empty' resonator LER 8. In the following, we analyze the spin-photon coupling derived from these experiments in a quantitative way.

The microwave transmission data were fitted using again Eq. (2). The results are shown in Fig. 6e-f. From these fits, we estimate G_N to both resonators

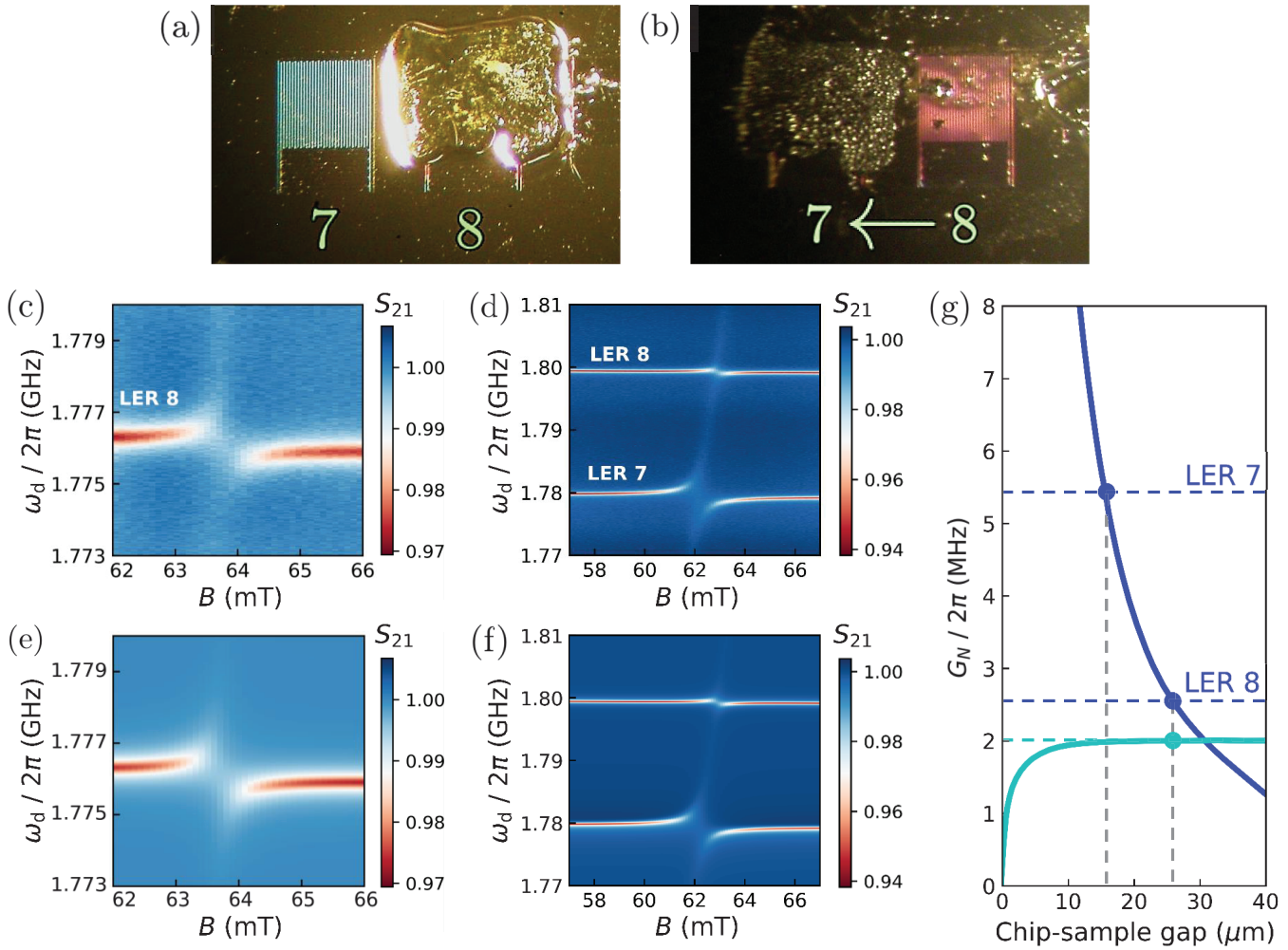

FIG. 6. **Spin-photon coupling of small DPPH grains located very close to the chip surface. a**: Optical microscopy images of LERs 7 and 8 of the chip sketched in figure 1b, with a DPPH sample deposited only on LER 8. **b**: The same sample has been transferred to LER 7, leaving behind a few small grains stuck on the oil layer on top of LER 8. **c**: Chip transmission for driving frequencies close to the resonance frequency ω_r of LER 8, measured for static magnetic fields around the spin-photon resonance condition $\omega_r = \omega_q = \mu_B g_S B_{res}/\hbar$ with a large DPPH sample on top of the resonator. **d**: Chip transmission for driving frequencies close to ω_r of LERs 7 and 8, measured for static magnetic fields around the spin-photon resonance condition $\omega_r = \omega_q = \mu_B g_S B_{res}/\hbar$ with the DPPH sample from LER 8 transferred to LER 7. **e-f**: Fit of the experimental data with Eq. (2). **g**: Collective spin-photon coupling generated by the inductor of LERs 7 and 8 calculated as a function of the gap that separates the sample from the chip surface (blue solid lines). The cyan solid line gives the spin-photon coupling $G_{N'}$ calculated for small DPPH grains covering a 5 % of the gap volume in LER 8 as a function of the gap thickness. The dots are the experimental G_N values obtained in the different experiments.

in the two experiments. We observe that $G_N/2\pi = 5.437 \pm 0.004$ MHz to LER 7 obtained from the second measurement is a factor of more than 2 higher than $G_N/2\pi = 2.555 \pm 0.004$ MHz to LER 8 that we get from the first one. Since the sample and the LER design are virtually the same in both experiments, this difference must be associated with the effect described in section III. The gap separating the sample from the chip surface gets smaller as some of the oil is lost during the sample transfer. Figure 6g, akin to Fig. 4b, shows that the change in G_N can be accounted for by decreasing the gap from about 26 μm to about 16 μm, which are close to the values found from the experiments performed with the first chip.

Let us now turn our attention to the results obtained for LER 8 in the second experiment. A first noticeable effect is that $\omega_r/2\pi$ increases by about 23 MHz after the sample has been removed from it (compare Figs. 6c and d). Experiments performed at zero magnetic field strongly suggest that this frequency shift arises from the relative permittivity $\epsilon > 1$ of the oil and of the DPPH sample. When they cover the LER, it leads to a larger capacitance, thus to a lower ω_r. Here, this effect is compatible with most of the sample and a good fraction of the

oil being removed from LER 8 when the sample is moved to LER 7, as the microscopy image Fig. 6b suggests.

Next, we consider the origin of the coupling to the 'empty' LER 8 that is obtained from the second experiment. We attribute it to the small amount of DPPH powder grains that remain stuck on the oil layer that remains just above it when the sample is moved to LER 7, and which are visible under the microscope (Fig. 6b). Comparing the area of the inductor covered by these grains with that of the original sample (100 % of the inductor), we estimate an upper bound $N/10$ to the number N' of remaining DPPH spins. Surprisingly at first, the spin-photon coupling associated to this fraction of the sample is higher than expected. As Fig. 6g shows, we get $G_{N'}/2\pi = 2.020 \pm 0.004$ MHz, that is, about 80 % of that obtained with the whole sample. This is more than two times larger than what one would expect by simply scaling the spin-photon coupling using the upper bound to N' ($G_{N'} = G_N\sqrt{N'/N} < G_N/\sqrt{10}$, which gives $G_{N'}/2\pi < 0.8$ MHz). This suggests that the small DPPH grains placed close to the resonator surface contribute more to the collective coupling than the remaining, and much larger, sample.

This idea can be tested with a toy model, whose basic features are sketched in Fig. 4a. When the sample is moved from LER 8 to its companion in the same pair, the DPPH grains that remain on LER 8 are those that were originally closest to the surface of the chip, likely embedded inside the oil gap. The simulation shown as a cyan line in Fig. 6g considers that about 5% of the original ~ 26 μm thick gap was occupied by DPPH molecules. In spite of its crude approximations, the results account very well for the spin-photon couplings measured before and after the sample was removed from this LER. They serve to underline the crucial role played by the spin location with respect to the circuit, which arises from the strong inhomogeneity of the resonator field.

VI. CONCLUSIONS

We have explored the coupling of free-radical molecular spin ensembles to the photon modes of lumped-element superconducting resonators. The collective coupling G_N of relatively large samples ($N \sim 10^{17}$) was found to be at least of the same order of the spin decoherence rate $\gamma_\perp$, reaching the high cooperativity regime for all resonators. In one case, the signatures that characterize the strong, or coherent, coupling regime ($G_N > \gamma_\perp$) between the spins and the photons, and the existence of hybrid polaritonic excitations were also observed. The results show also that the spin-photon coupling can be tuned, in situ, by modifying the orientation of the magnetic field that polarizes the molecular spins. In this way, we have been able to detect the direct coupling of the spins to the transmission line. Taken together, these results show that these circuits provide a suitable basis for combining a broadband control of the spin states with the possibility of dispersively reading out the results; i.e. they provide the basic ingredients for performing the basic operations of a hybrid molecular spin quantum processor.[26]

Our study has also revealed the very important, in this case dominant effect that the location of the spins has on their interaction with the microwave photons. Due to the inherently inhomogenous distribution of the microwave magnetic field that the LERs generate, the attainable coupling is, to a large extent, determined by how closely the sample can be placed above the surface of the chip. The need of fixing, and thermalizing, the samples with the help of some intermediate agent, in our case paratone oil, limits the maximum coupling that can be achieved in practice. Our results provide also some practical tricks to minimize this effect when dealing with macroscopic molecular samples. Still, it is clear that fully exploiting the possibilities offered by lumped element resonators to maximize their coupling to molecular spins, e.g. by reducing their impedance and/or their mode volume,[39–42] must go hand in hand with methods that allow optimizing the chip-molecules interface. The results show that this second aspect can contribute very significantly to enhance the coupling to very small spin ensembles.

The fact that many molecular nanomagnets are stable in solution provides an alternative to the use of bulk samples. The combination of this method and of soft nanolithography techniques with a high spatial resolution, like Dip Pen Nanolithography, has enabled reaching very high single spin-photon couplings with coplanar superconducting resonators.[43] However, this idea is only applicable whenever the molecular orientation does not play a major role, e.g. when one deals with isotropic spins such as those in DPPH. The case of anisotropic molecular spins, which are very interesting to encode spin qudits, requires a different approach. Interesting possibilities are based on the application of molecular self-organization techniques, which can be assisted by previously deposited mono-layers of non-magnetic molecules acting as grafting centers,[44] or by employing chemical tools that allow transferring a preformed molecular lattice onto the device.[45] In these cases, the strong inhomogeneity of the microwave magnetic field can be advantageously exploited to address certain molecular spins from the lattice, via a proper circuit design, thus helping to circumvent the need of positioning the molecules one by one. Even though still challenging, the results suggest that lumped element resonators are very promising for the control and readout of molecular spin qubits.

ACKNOWLEDGMENTS

This work has received support from grants TED2021-131447B-C21, TED2021-131447B-C22, PID2022-140923NB-C21, and CEX2020-001039-S, funded by MCIN/AEI/10.13039/501100011033, ERDF 'A way of making Europe' and ESF 'Investing in your future', from the Gobierno de Aragón grant E09-23R-Q-MAD and the

'Severo Ochoa' Programme for Centres of Excellence in R&D (CEX2020-001039-S). This study forms also part of the Advanced Materials and Quantum Communication programmes, supported by MCIN with funding from European Union NextGenerationEU (PRTR-C17.I1), by Gobierno de Aragón, and by CSIC (PTI001).

[1] A. Gaita-Ariño, F. Luis, S. Hill, and E. Coronado, Nature Chemistry **11**, 1755 (2019).
[2] M. Atzori and R. Sessoli, J. Am. Chem. Soc. **141**, 11339–11352 (2019).
[3] M. R. Wasielewski, M. D. E. Forbes, N. L. Frank, K. Kowalski, G. D. Scholes, J. Yuen-Zhou, M. A. Baldo, D. E. Freedman, R. H. Goldsmith, T. Goodson III, M. L. Kirk, J. K. McCusker, J. P. Ogilvie, D. A. Shultz, S. Stoll, and K. B. Whaley, Nature Reviews Chemistry **4**, 490 (2020).
[4] C. J. Wedge, G. A. Timco, E. T. Spielberg, R. E. George, F. Tuna, S. Rigby, E. J. L. McInnes, R. E. P. Winpenny, S. J. Blundell, and A. Ardavan, Phys. Rev. Lett. **108**, 107204 (2012).
[5] K. Bader, D. Dengler, S. Lenz, B. Endeward, S.-D. Jiang, P. Neugebauer, and J. van Slageren, Nat. Commun **5**, 5304 (2014).
[6] J. M. Zadrozny, J. Niklas, O. G. Poluektov, and D. E. Freedman, ACS Cent. Sci. **1**, 488 (2015).
[7] M. Shiddiq, D. Komijani, Y. Duan, A. Gaita-Ariño, E. Coronado, and S. Hill, Nature **531**, 348 (2016).
[8] K. Kundu, J. Chen, S. Hoffman, J. Marbey, D. Komijani, Y. Duan, A. Gaita-Ariño, J. Stanton, X. Zhang, C. Hai-Ping, and S. Hill, Commun. Phys. **6**, 38 (2023).
[9] F. Luis, A. Repollés, M. J. Martínez-Pérez, D. Aguilà, O. Roubeau, D. Zueco, P. J. Alonso, M. Evangelisti, A. Camón, J. Sesé, L. A. Barrios, and G. Aromí, Phys. Rev. Lett. **107**, 117203 (2011).
[10] G. Aromí, D. Aguilà, P. Gamez, F. Luis, and O. Roubeau, Chem. Soc. Rev. **41**, 537 (2012).
[11] D. Aguilà, L. A. Barrios, V. Velasco, O. Roubeau, A. Repollés, P. J. Alonso, J. Sesé, S. J. Teat, F. Luis, and G. Aromí, J. Am. Chem. Soc. **136**, 14215 (2014).
[12] A. Fernández, J. Ferrando-Soria, E. Moreno-Pineda, F. Tuna, I. J. Vitorica-Yrezabal, C. Knappke, J. Ujma, C. A. Muryn, G. A. Timco, P. E. Barran, A. Ardavan, and R. E. P. Winpenny, Nat. Commun. **7**, 10240 (2016).
[13] J. Ferrando-Soria, E. Moreno-Pineda, A. Chiesa, A. Fernández, S. A. Magee, S. Carretta, P. Santini, I. J. Vitorica-Yrezabal, F. Tuna, G. A. Timco, E. J. L. McInnes, and R. E. P. Winpenny, Nat. Commun. **7**, 11377 (2016).
[14] M. D. Jenkins, Y. Duan, B. Diosdao, J. J. García-Ripoll, A. Gaita-Ariño, C. Giménez-Saiz, P. J. Alonso, E. Coronado, and F. Luis, Phys. Rev. B **95**, 064423 (2017).
[15] C. Godfrin, A. Ferhat, R. Ballou, S. Klyatskaya, M. Ruben, W. Wernsdorfer, and F. Balestro, Phys. Rev. Lett. **119**, 187702 (2017).
[16] R. Hussain, G. Allodi, A. Chiesa, E. Garlatti, D. Mitcov, A. Konstantatos, K. S. Pedersen, R. De Renzi, S. Piligkos, and S. Carretta, J. Am. Chem. Soc. **140**, 9814 (2018).
[17] E. Moreno-Pineda, C. Godfrin, F. Balestro, W. Wernsdorfer, and M. Ruben, Chem. Soc. Rev. **47**, 501 (2018).
[18] F. Luis, P. J. Alonso, O. Roubeau, V. Velasco, D. Zueco, D. Aguilà, J. I. Martínez, L. A. Barrios, and G. Aromí, Communications Chemistry **3**, 176 (2020).
[19] S. Carretta, D. Zueco, A. Chiesa, A. Gómez-León, and F. Luis, Appl. Phys. Lett. **118**, 240501 (2021).
[20] A. Blais, R.-S. Huang, A. Wallraff, S. M. Girvin, and R. J. Schoelkopf, Physical Review A **69**, 062320 (2004).
[21] A. Wallraff, D. I. Schuster, A. Blais, L. Frunzio, R.-S. Huang, J. Majer, S. Kumar, S. M. Girvin, and R. J. Schoelkopf, Nature **431**, 162 (2004).
[22] J. Majer, J. M. Chow, J. M. Gambetta, J. Koch, B. R. Johnson, J. A. Schreier, L. Frunzio, D. I. Schuster, A. A. Houck, A. Wallraff, A. Blais, M. H. Devoret, S. M. Girvin, and R. J. Schoelkopf, Nature **449**, 443 (2007).
[23] J. Schoelkopf and S. M. Girvin, Nature **451**, 664 (2008).
[24] M. D. Jenkins, T. Hümmer, M. J. Martínez-Pérez, J. J. García-Ripoll, D. Zueco, and F. Luis, New Journal of Physics **15**, 095007 (2013).
[25] M. D. Jenkins, D. Zueco, O. Roubeau, G. Aromi, J. Majer, and F. Luis, Dalton Transactions **45**, 16682 (2016).
[26] A. Chiesa, S. Roca, S. Chicco, M. de Ory, A. Gómez-León, A. Gomez, D. Zueco, F. Luis, and S. Carretta, Phys. Rev. Appl. **19**, 064060 (2023).
[27] A. Gómez-León, F. Luis, and D. Zueco, Phys. Rev. Applied **17**, 064030 (2022).
[28] A. Gómez-León, Phys. Rev. A **106**, 022609 (2022).
[29] M. Göppl, A. Fragner, M. Baur, R. Bianchetti, S. Filipp, J. M. Fink, P. J. Leek, G. Puebla, L. Steffen, and A. Wallraff, Journal of Applied Physics **104**, 113904 (2008).
[30] A. Ghirri, C. Bonizzoni, F. Troiani, N. Buccheri, L. Beverina, A. Cassinese, and M. Affronte, Physical Review A **93**, 063855 (2016).
[31] C. Bonizzoni, A. Ghirri, M. Atzori, L. Sorace, R. Sessoli, and M. Affronte, Scientific Reports **7**, 13096 (2017).
[32] M. Mergenthaler, J. Liu, J. J. L. Roy, N. Ares, A. L. Thompson, L. Bogani, F. Luis, S. J. Blundell, T. Lancaster, A. Ardavan, G. A. D. Briggs, P. J. Leek, and E. A. Laird, Physical Review Letters **119**, 147701 (2017).
[33] S. Weichselbaumer, M. Zens, C. W. Zollitsch, M. S. Brandt, S. Rotter, R. Gross, and H. Huebl, Physical Review Letters **125**, 137701 (2020).
[34] N. D. Yordanov, Applied Magnetic Resonance **10**, 339 (1996).
[35] D. Z. Žilić, D. Pajić, M. Jurić, K. Molčanov, B. Rakvin, P. Planinić, and K. Zadro, Journal of Magnetic Resonance **207**, 34 (2010).
[36] C. A. González-Gutiérrez, D. García-Pons, D. Zueco, and M. J. Martínez-Pérez, arXiv preprint arXiv:2401.06549 (2024).
[37] V. Rollano, M. C. de Ory, C. D. Buch, M. Rubín-Osanz, D. Zueco, C. Sánchez-Azqueta, A. Chiesa, D. Granados, S. Carretta, A. Gomez, S. Piligkos, and F. Luis, Communications Physics **5**, 246 (2022).
[38] A. Castro, A. García Carrizo, S. Roca, D. Zueco, and F. Luis, Phys. Rev. Appl. **17**, 064028 (2022).
[39] A. Bienfait, A. A. Pla, Y. Kubo, X. Stern, M. Zhou, C. C. Lo, C. D. Weis, T. Schenkel, M. L. W. Thewalt, D. Vion, D. Esteve, B. Julsgaard, K. Mølmer, J. J. L. Morton, and P. Bertet, Nature Nanotech. **11**, 253 (2016).

[40] S. Probst, A. Bienfait, P. Campagne-Ibarcq, J. J. Pla, B. Albanese, J. F. Da Silva Barbosa, T. Schenkel, D. Vion, D. Esteve, K. Mølmer, J. J. L. Morton, R. Heeres, and P. Bertet, Appl. Phys. Lett. **111**, 202604 (2017).
[41] C. Eichler, A. J. Sigillito, S. A. Lyon, and J. R. Petta, Phys. Rev. Lett. **118**, 037701 (2017).
[42] B. Sarabi, P. Huang, and N. M. Zimmerman, Phys. Rev. Applied **11**, 014001 (2019).
[43] I. Gimeno, W. Kersten, M. C. Pallarés, P. Hermosilla, M. J. Martínez-Pérez, M. D. Jenkins, A. Angerer, C. Sánchez-Azqueta, D. Zueco, J. Majer, A. Lostao, and F. Luis, ACS Nano **14**, 8707– (2020).
[44] L. Tesi, F. Stemmler, M. Winkler, S. S. Y. Liu, S. Das, X. Sun, M. Zharnikov, S. Ludwigs, and J. van Slageren, Advanced Materials **35**, 2208998 (2023).
[45] A. Urtizberea, E. Natividad, P. J. Alonso, L. Pérez-Martínez, M. A. Andrés, I. Gascón, I. Gimeno, F. Luis, and O. Roubeau, Mater. Horiz. **7**, 885 (2020).